Oblique Breathers Generated by a Flow of Two-Component Bose-Einstein Condensates Past a Polarized Obstacle

A. M. Kamchatnov and Y. V. Kartashov

Institute of Spectroscopy, Russian Academy of Sciences, Troitsk, Moscow, 142190, Russia

(Received 6 August 2013; published 3 October 2013)

We predict that oblique breathers can be generated by a flow of two-component Bose-Einstein condensates past a polarized obstacle that attracts one component of the condensate and repels the other one. The breather exists if intraspecies interaction constants differ from the interspecies interaction constant, and it corresponds to the nonlinear excitation of the so-called polarization mode with domination of the relative motion of the components. Analytical theory is developed for the case of small-amplitude breathers that is in reasonable agreement with the numerical results.

DOI: 10.1103/PhysRevLett.111.140402 PACS numbers: 03.75.Lm, 03.75.Kk, 03.75.Mn

Introduction.—The flow of Bose-Einstein condensates (BECs) past obstacles reveals a number of different nonlinear excitations of the condensate. For example, in a one-component condensate with the sound velocity c_s the flow is superfluid for velocities V satisfying the condition $M \equiv V/c_s < M_c$ ($M_c \approx 0.37$ for the flow past a disk in two-dimensional geometry). For greater Mach numbers $M > M_c$, vortices are generated by the flow, which means loss of superfluidity [1–5]. Another channel of dissipation opens, according to the Landau criterion, when the flow velocity exceeds the sound velocity, that is, at $M = 1$ [6,7]. In this case, the interference of Bogoliubov waves generated by a supersonic flow leads to formation of a so-called ''ship-wave'' pattern located outside the Mach cone [8,9]. Inside the Mach cone, the vortex streets are generated in the flow velocity interval $1 < M < 1.44$, but for velocities with $M > 1.44$, very specific oblique dark solitons [10] are generated [11–13]. They have been observed in experiments [14,15] with flows of polariton condensates past obstacles. These nonlinear structures manifest themselves as dips in the distributions of the condensate's density.

The creation of two-component atomic [16,17] and spinor polariton [18,19] condensates triggered extensive research activity, both theoretical and experimental, centered around the nonlinear properties of two-species superfluids [20,21]. One of the new properties of such superfluids is the possibility of formation of topological excitations [22,23]. Another specific feature of two-species superfluids is the existence of two modes of motion that can be called *density* and *polarization* waves—in the density waves the two species move mainly in phase with each other whereas in the polarization waves they move mainly in counter phase. In the linear limit, there exist, correspondingly, two types of sound waves, which in problems such as a description of wave patterns generated by the flow past an obstacle define two Mach cones and two types of ship waves. The existence of two different types of excitations in such a condensate suggests the possibility of two different types of oblique dark solitons that may be generated upon the interaction of condensate with a defect. However, previously only one type of oblique dark soliton [24] has been observed in the flow past a nonpolarized obstacle, i.e., the obstacle whose potential acts equally on both species of the condensate. Such potential disturbs both species ''in phase,'' thereby exciting only density waves with symmetry similar to that of the potential. This suggests that another, previously elusive, polarization mode can be generated by a *polarized* obstacle that acts differently on different species of the condensate. Such an obstacle can be realized by generalization of the method used in the experiments described in Ref. [8]. As is known [25], a laser beam with a blue-detuned light frequency with respect to the resonance atomic optical transition creates a repulsive potential of the gradient force acting on atoms, and such a beam was used in Ref. [8] for the formation of a cylindrical obstacle that acted on the condensate flowing past it. If the optical transitions from the states of atoms in different species of a two-component condensate have frequencies at different sides of the laser beam frequency, then such a beam will be blue detuned for one component and red detuned for another component. Hence, the gradient forces will have opposite signs for different condensate components, and such a beam will act as a polarized obstacle.

In this Letter, we study the properties of wave patterns generated by the two-dimensional flow of a two-component condensate past such a polarized obstacle and demonstrate that in this case a previously unknown type of excitation enters the scene—an *oblique breather*. One of the most distinctive features of such breathers is that in contrast to conventional dark-dark solitons generated by nonpolarized potentials, the density distributions in two components of the breather have different shapes with deep out-of-phase modulation. The properties of oblique breathers are studied numerically using two coupled Gross-Pitaevskii (GP) equations and explained analytically in the small-amplitude limit by reducing the GP system to a modified Korteweg–de Vries (MKdV) equation for a weakly nonlinear polarization mode.

The model.—In the mean field theory, the dynamics of two-component BEC is described by the system of GP equations in standard nondimensional form

$$i\frac{\partial\psi_1}{\partial t}+\frac{1}{2}\Delta\psi_1-(g_{11}|\psi_1|^2+g_{12}|\psi_2|^2)\psi_1=\sigma_1U(\mathbf{r})\psi_1,$$
$$i\frac{\partial\psi_2}{\partial t}+\frac{1}{2}\Delta\psi_2-(g_{12}|\psi_1|^2+g_{22}|\psi_2|^2)\psi_2=\sigma_2U(\mathbf{r})\psi_2, \quad (1)$$

where Laplacian Δ acts on two spatial coordinates $\mathbf{r}=(x,y)$. We assume that the potential $\sigma_kU(\mathbf{r},t)$ of the obstacle is repulsive if $\sigma_k=1$ and attractive if $\sigma_k=-1$. In our simulations, it is modeled by the form $U(\mathbf{r})=U_0\exp(-\mathbf{r}^2/a^2)$ with $U_0=1.0$, $a=2$. The nonlinear interaction constants g_{ik} are positive. We assume that both components have in an undisturbed uniform state the same densities $\rho_1=\rho_2=\rho_0/2$, where $\rho_1=|\psi_1|^2$, $\rho_2=|\psi_2|^2$, and ρ_0 is an undisturbed total density $\rho=\rho_1+\rho_2$ at $|\mathbf{r}|\to\infty$.

Linearization of the system (1) for a slightly disturbed background state yields the dispersion relations for the linear waves in the two-component condensate (see, e.g., Ref. [24]) $\omega_{d,p}^2=c_{d,p}^2k^2+\frac{1}{4}k^4$, where

$$c_{d,p}=\frac{1}{2}(\rho_0\{g_{11}+g_{22}\pm[(g_{11}-g_{22})^2+4g_{12}^2]^{1/2}\})^{1/2}$$

are the velocities of the density (c_d, upper sign) and polarization (c_p, lower sign) waves, whereas $\omega_{d,p}$ are the frequencies describing the temporal evolution of perturbations $\propto\exp(-i\omega_{d,p}t)$. The presence of two different velocities leads to the existence of two Mach cones defined by the relations

$$\sin\chi_{d,p}=\frac{c_{d,p}}{V}\equiv\frac{1}{M_{d,p}}, \quad (2)$$

where $M_{d,p}=V/c_{d,p}$ are the corresponding Mach numbers; $\chi_{d,p}$ are the angles between the direction of the flow and the lines representing the *density* and *polarization* cones.

Oblique breathers.—In order to demonstrate the principal difference between wave patterns generated by nonpolarized ($\sigma_1=\sigma_2=1$) and polarized ($\sigma_1=-\sigma_2=1$) obstacles, we solved the system (1) numerically for these two cases using the input conditions $\psi_{1,2}=(\rho_0/2)^{1/2}\times\exp(iVx)$. Typical results are illustrated in Fig. 1. For the nonpolarized obstacle the density ship waves are located outside the density Mach cone, and a dark-dark soliton is located inside it. Remarkably, the existence of the polarization Mach cone is not manifested at all in the density distributions of both condensate components—polarization waves are not excited by the nonpolarized obstacle. In sharp contrast, the polarized obstacle leads to much richer dynamics and generates both density ship waves (outside the outer Mach cone) and polarization ship waves

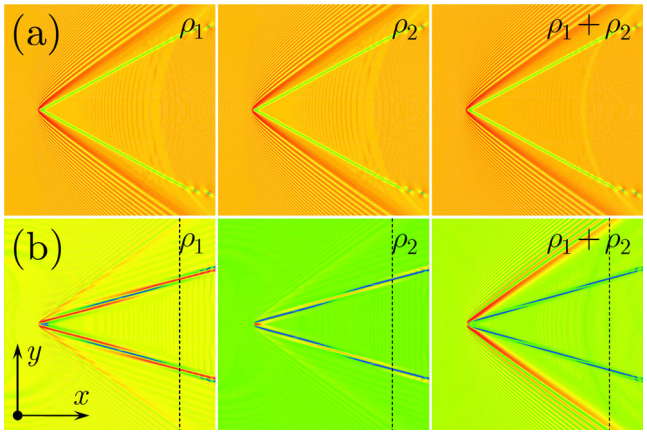

FIG. 1 (color online). Distributions of the densities of the first (left column) and second (central column) components, as well as of total density (right column) for (a) nonpolarized obstacle with $\sigma_1=\sigma_2=1$, and for (b) polarized obstacle with $\sigma_1=1$, $\sigma_2=-1$. In both cases $g_{11}=g_{22}=1.0$, $g_{12}=0.6$, $V=2.3$, and $t=160$. Here and in Figs. 3 and 5 blue regions in the color map indicate locations where density of the condensate is minimal, while red regions correspond to highest densities.

(outside the inner Mach cone). The density waves oscillate in phase in both components that increases the amplitude of oscillations in the total density, whereas the counterphase oscillations in the condensate components in the polarization ship waves lead to cancellation of oscillations in the total density. The polarized obstacle does not excite a usual dark-dark soliton, but instead a more complicated structure is generated in the vicinity of the polarization Mach cone. We shall call this structure an *oblique breather* since it can be related with time-dependent breather solutions of the associated nonlinear evolution equations.

More detailed structure of the wave pattern generated by the polarized obstacle can be seen in Fig. 2 representing the density distributions along the y axis at fixed value of x coordinate. The oblique breather can be represented as a modulated nonlinear wave with counterphase nonlinear oscillations of the condensate components. When its envelope is much narrower than the distance between two Mach cones, the space between the oblique breather and the density ship waves is occupied by the polarization ship waves clearly visible in Figs. 1 and 2. The parameters of the oblique breather are determined by the parameters of the incoming flow and those of the obstacle. The complete cancellation of oscillations of the components in the total density distribution occurs only if $g_{11}=g_{22}$; otherwise, the linear eigenmodes correspond to a mixture of pure density and polarization waves [26]. The most important control parameter is the incoming flow velocity V. In Fig. 3 we illustrate the modifications in the wave pattern generated by the flow past a polarized obstacle with growth of V. If $V=1.3$, then the breather is absolutely unstable, and one observes the formation of vortex streets. If $V=1.9$, then a clearly resolvable breather is formed, and further

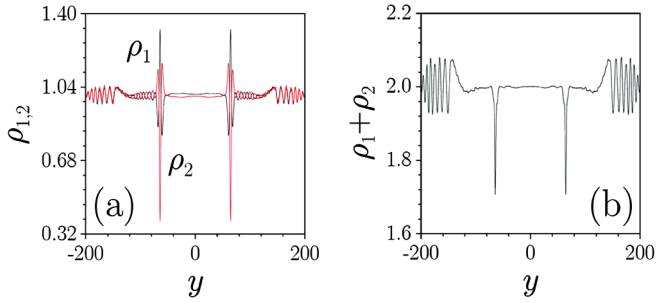

FIG. 2 (color online). The distributions of densities in two components (a) and total density (b) along the y axis at $x = 100$, $t = 160$ [these distributions correspond to the dashed lines in Fig. 1(b)].

increase of velocity to $V = 2.3$ changes only its inclination angle with respect to the direction of the flow but does not essentially change its parameters. We suppose that this transition from a nonstationary vortex emission to a stationary formation of oblique breather is physically similar to the transition from absolute instability of oblique dark solitons to their convective instability studied in Refs. [12,13,27] for the one-component BEC flow.

Analytical theory.—Although the exact breather solutions of Eqs. (1) are unknown, we develop here the approximate theory for the small-amplitude breathers that explains with reasonable accuracy the observed features of new wave structures. To this end, we consider a one-dimensional version of the system (1) that describes waves

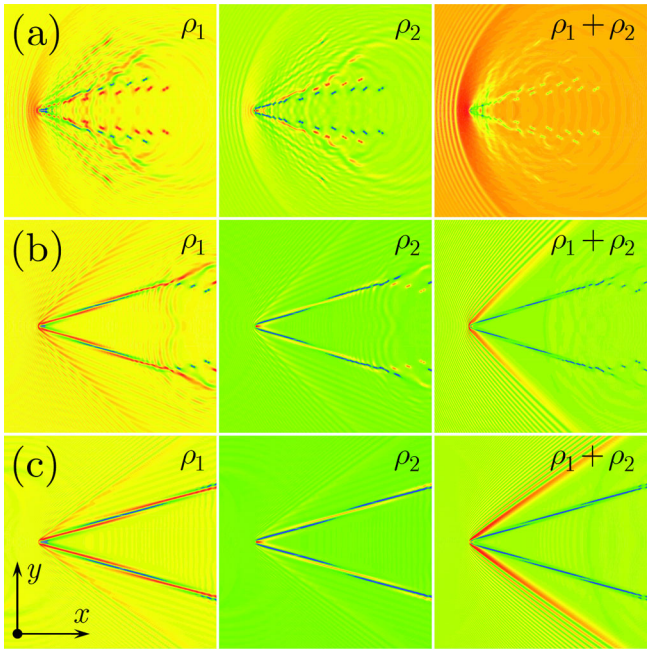

FIG. 3 (color online). Distributions of the densities of the first (left column) and second (central column) components as well as of total density (right column) at $t = 160$ for the velocity of the flow $V = 1.3$ (a), $V = 1.9$ (b), and $V = 2.3$ (c). In all cases, $g_{11} = g_{22} = 1.0$, $g_{12} = 0.6$.

propagating along the x' axis. For the separation of density and polarization modes, it is convenient to introduce a spinor representation of the field variables [28]

$$\begin{pmatrix} \psi_1 \\ \psi_2 \end{pmatrix} = \sqrt{\rho} e^{i\Phi/2} \chi = \sqrt{\rho} e^{i\Phi/2} \begin{pmatrix} \cos\frac{\theta}{2} e^{-i\phi/2} \\ \sin\frac{\theta}{2} e^{i\phi/2} \end{pmatrix}, \quad (3)$$

where Φ has the meaning of the velocity potential of the in-phase motion; the angle θ is the variable describing the relative density of the two components [$\cos\theta = (\rho_1 - \rho_2)/\rho$], and ϕ is the potential of the relative counterphase motion. The densities of the condensate components are given by $\rho_1 = \rho\cos^2(\theta/2)$, $\rho_2 = \rho\sin^2(\theta/2)$. In the uniform quiescent state of BEC with equal densities in the components, we can take $\theta = \theta_0 = \pi/2$ and then the small-amplitude waves correspond to small variations of the relative density variable $\theta' \equiv \theta - \theta_0$ and small in-phase $U = \Phi_{x'}$ and counterphase $v = \phi_{x'}$ velocities. The perturbation theory [26] for polarization waves with account of small dispersion and weak nonlinearity yields then the evolution equation, which for $g_{11} = g_{22} \neq g_{12}$ has the form of the MKdV equation for θ':

$$\theta'_t + c_p\theta'_{x'} - \frac{3c_p(9g_{11} - g_{12})}{8g_{12}}\theta'^2\theta'_{x'} - \frac{1}{8c_p}\theta'_{x'x'x'} = 0. \quad (4)$$

If its solution is found, then the other field variables are expressed in terms of θ' by the formulas

$$\rho = \rho_0 - \frac{3c_p^2}{2g_{12}}\theta'^2, \quad U = -\frac{c_p(3g_{11} + g_{12})}{2g_{12}}\theta'^2, \quad v = 2c_p\theta'. \quad (5)$$

The MKdV Eq. (4) has a variety of solutions, among which there is the one-dimensional breather solution, presented in Ref. [29], which in our notations can be written as

$$\theta' = -\frac{2}{c_p}\sqrt{\frac{2g_{12}}{9g_{11} - g_{12}}}\frac{\partial}{\partial x'}\arctan\left(\frac{\eta\cos(\Theta_1 + \beta_1)}{\xi\cosh(\Theta_2 + \beta_2)}\right), \quad (6)$$

where

$$\begin{aligned} \Theta_1 &= 2\xi(x' - c_pt) - \xi(\xi^2 - 3\eta^2)t/c_p, \\ \Theta_2 &= 2\eta(x' - c_pt) - \eta(3\xi^2 - \eta^2)t/c_p, \\ \xi &= \kappa\cos q, \qquad \eta = \kappa\sin q, \\ \beta_1 &= p - q, \qquad \beta_2 = \ln(2\kappa\tan q/a), \end{aligned} \quad (7)$$

and p, q, κ, a are free parameters. This solution gives an approximate description of the oblique breather pattern found above numerically when it is transformed to the appropriate reference frame and the parameters are chosen in a proper way. The solution (6) is written in the reference frame associated with a quiescent condensate, where the breather propagates with the envelope velocity $V_b = c_p + (3\xi^2 - \eta^2)/(2c_p)$ and the carrier wave velocity $V_c = c_p + (\xi^2 - 3\eta^2)/(2c_p)$ along the x' axis with the breather

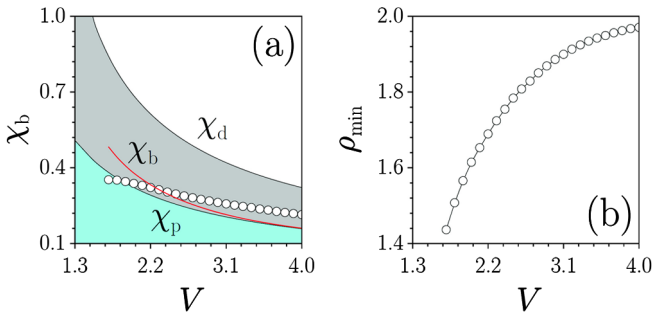

FIG. 4 (color online). The inclination angle χ (a) and depth $\rho_{min} = \rho_0 - \Delta\rho$ (b) of the oblique breather generated by the flow of condensate past the polarized obstacle versus flow velocity V at $g_{11} = g_{22} = 1.0$, $g_{12} = 0.6$. In (a), the line with circles shows numerical results, whereas the red solid line shows the analytical prediction (8) for the inclination angle. The blue region corresponds to the inner Mach cone, whereas the region between inner and outer Mach cones is shown in gray.

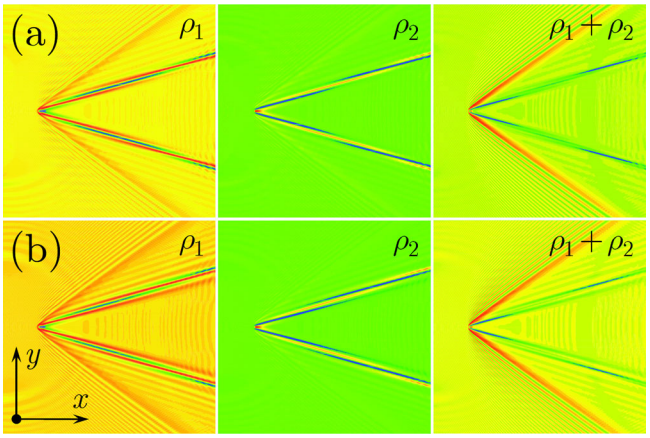

FIG. 5 (color online). Density distributions generated by the polarized obstacle at (a) $g_{11} = 1.1$, $g_{22} = 0.9$ and (b) $g_{11} = 1.2$, $g_{22} = 0.8$. In both cases, $V = 2.3$, $t = 160$, and $g_{12} = 0.6$.

location line parallel to the y' axis. We must transform it to the reference frame with the obstacle located at the axes origin, the condensate's flow velocity directed along the x axis, and the breather location line inclined with respect to the x axis at some angle χ_b chosen in such a way that the breather becomes a stationary structure in the new reference frame. The same transformation must compensate both the envelope velocity and the carrier wave velocity, $V_b = V_c$, what gives $q = \pi/4$. Besides that, these two velocities must be compensated by the projection of the flow velocity $V\sin\chi_b$ on the x' axis. This can be realized only at $c_p + \kappa^2/(2c_p) = V\sin\chi_b$. After these transformations, the phases Θ_1 and Θ_2 must be replaced by $\Theta_1 = \Theta_2 = \sqrt{2}\kappa\cos\chi_b(y \pm x\tan\chi_b)$ and, as a result, the solution Eq. (6) transforms into the distribution of θ' in the (x, y) plane. Substitution of $\theta'(x, y)$ into Eqs. (7) yields the distributions of the other field variables.

It is convenient to express the parameter κ in terms of the maximal amplitude of the density envelope $\Delta\rho \equiv |\rho - \rho_0| = 24\kappa^2/(9g_{11} - g_{12})$. As a result, we get, with account of the expression $c_p^2 = \rho_0(g_{11} - g_{12})/2$, which is valid if $g_{11} = g_{22}$, a useful relation between the breather angle χ_b and the maximal envelope amplitude $\Delta\rho$

$$\sin\chi_b = \frac{1}{M_p}\left(1 + \frac{9g_{11} - g_{12}}{24(g_{11} - g_{12})}\frac{\Delta\rho}{\rho_0}\right). \qquad (8)$$

Importantly, this formula predicts that the oblique breathers are located outside the polarization Mach cone defined by Eq. (2). Another important relation is given by the dependence of the inverse width $w = 4\eta$ of the breather on its amplitude $\Delta\rho$, $w = \sqrt{(9g_{11} - g_{12})\Delta\rho/3}$.

Numerically found dependence of the breather angle χ_b as a function of V is shown in Fig. 4(a) by circles. As one can see, it agrees with qualitative prediction that oblique breathers are located outside the polarization Mach cone. For comparison with the analytical formula (8) we determined numerically the minimal density $\rho_{min} = \rho_0 - \Delta\rho$ in the breather as a function of V which is plotted in Fig. 4(b). Substitution of this $\Delta\rho$ into Eq. (8) yields the dependence of χ_b on V which is shown in Fig. 4(a) by a red line. It perfectly agrees with numerical values of χ_b at velocities close to $V \approx 2$, however, the theoretical dependence deviates from the numerical one for $V \gtrsim 3$. We explain this disagreement by the fact that at $V \simeq 3$ the breather's width is of the same order as the distance between the two Mach cones and the breather cannot be considered as a structure well separated from other excitations.

The above theory was developed for the case when $g_{11} = g_{22}$. It is of considerable interest to study what happens if $g_{11} \neq g_{22}$. Corresponding results obtained by direct solution of Eqs. (1) are presented in Fig. 5. Now the counterphase oscillations of the densities of components do not compensate each other, and the ship-wave pattern becomes clearly visible in the distribution of the total density. With increase of the difference $g_{11} - g_{22}$, the width of the oblique breathers also increases, but qualitatively the whole wave pattern remains the same. The appearance of the density ship wave indicates a strong mixing of the density and polarization modes. One could expect that in situations with strong mixing of these two modes due to spin-orbit coupling [30] the breatherlike excitations could also be generated by a nonpolarized obstacle. We have studied this situation numerically and found that an account of the spin-orbit coupling changes the conditions for generation of these wave structures, but the flow past a nonpolarized obstacle still generates the oblique solitons and the flow past a polarized obstacle generates the oblique breathers.

Summarizing, we have predicted that new nonlinear structures—oblique breathers—can be generated by a flow of two-component condensates past polarized obstacles.

[1] T. Frisch, Y. Pomeau, and S. Rica, Phys. Rev. Lett. **69**, 1644 (1992).
[2] T. Winiecki, J. F. McCann, and C. S. Adams, Phys. Rev. Lett. **82**, 5186 (1999).
[3] N. G. Berloff and P. H. Roberts, J. Phys. A **33**, 4025 (2000).
[4] S. Rica, Physica (Amsterdam) **148D**, 221 (2001).
[5] C.-T. Pham, C. Nore, and M.-É. Brachet, Physica (Amsterdam) **210D**, 203 (2005).
[6] D. L. Kovrizhin and L. A. Maksimov, Phys. Lett. A **282**, 421 (2001).
[7] G. E. Astrakharchik and L. P. Pitaevskii, Phys. Rev. A **70**, 013608 (2004).
[8] I. Carusotto, S. X. Hu, L. A. Collins, and A. Smerzi, Phys. Rev. Lett. **97**, 260403 (2006).
[9] Yu. G. Gladush, G. A. El, A. Gammal, and A. M. Kamchatnov, Phys. Rev. A **75**, 033619 (2007).
[10] Y. S. Kivshar and B. Luther-Davies, Phys. Rep. **298**, 81 (1998).
[11] G. A. El, A. Gammal, and A. M. Kamchatnov, Phys. Rev. Lett. **97**, 180405 (2006).
[12] A. M. Kamchatnov and L. P. Pitaevskii, Phys. Rev. Lett. **100**, 160402 (2008).
[13] A. M. Kamchatnov and S. V. Korneev, Phys. Lett. A **375**, 2577 (2011).
[14] A. Amo, S. Pigeon, D. Sunvitto, V. G. Sala, R. Hivet, I. Carusotto, F. Pisanello, G. Leménager, R. Houdré, E. Giacobino, C. Ciuti, and A. Bramati, Science **332**, 1167 (2011).
[15] G. Grosso, G. Nardin, F. Morier-Genoud, Y. Léger, and B. Deveaud-Plédran, Phys. Rev. Lett. **107**, 245301 (2011).
[16] C. J. Myatt, E. A. Burt, R. W. Ghrist, E. A. Cornell, and C. E. Wieman, Phys. Rev. Lett. **78**, 586 (1997).
[17] D. M. Stamper-Kurn, M. R. Andrews, A. P. Chikkatur, S. Inouye, H.-J. Miesner, J. Stenger, and W. Ketterle, Phys. Rev. Lett. **80**, 2027 (1998).
[18] J. Kasprzak, M. Richard, S. Kundermann, A. Baas, P. Jeambrun, J. M. J. Keeling, F. M. Marchetti, M. H. Szymanska, R. André, J. L. Staehli, V. Savona, P. B. Littlewood, B. Deveaud, and L. S. Dang, Nature (London) **443**, 409 (2006).
[19] R. Balili, V. Hartwell, D. Snoke, L. Pfeiffer, and K. West, Science **316**, 1007 (2007).
[20] D. J. Frantzeskakis, J. Phys. A **43**, 213001 (2010).
[21] I. Carusotto and C. Ciuti, Rev. Mod. Phys. **85**, 299 (2013).
[22] H. Flayac, D. D. Solnyshkov, and G. Malpuech, Phys. Rev. B **83**, 193305 (2011).
[23] R. Hivet, H. Flayac, D. D. Solnyshkov, D. Tanese, T. Boulier, D. Andreoli, E. Giacobino, J. Bloch, A. Bramati, G. Malpuech, and A. Amo, Nat. Phys. **8**, 724 (2012).
[24] Yu. G. Gladush, A. M. Kamchatnov, Z. Shi, P. G. Kevrekidis, D. J. Frantzeskakis, and B. A. Malomed, Phys. Rev. A **79**, 033623 (2009).
[25] V. I. Balykin, V. G. Minogin, and V. S. Letokhov, Rep. Prog. Phys. **63**, 1429 (2000).
[26] A. M. Kamchatnov, Y. V. Kartashov, P.-É. Larré, and N. Pavloff, arXiv:1308.0784.
[27] M. A. Hoefer and B. Ilan, Multiscale Model. Simul. **10**, 306 (2012).
[28] K. Kasamatsu, M. Tsubota, and M. Ueda, Phys. Rev. A **71**, 043611 (2005).
[29] M. Wadati, J. Phys. Soc. Jpn. **34**, 1289 (1973).
[30] Q. Zhu, C. Zhang, and B. Wu, Europhys. Lett. **100**, 50003 (2012).